PROCEEDINGS OF SCIENCE

CALET on the International Space Station: new direct measurements of cosmic-ray iron and nickel

Francesco Stolzi,[a,b,*] **Caterina Checchia,**[a,b] **Gabriele Bigongiari**[a,b] **and Yosui Akaike**[c,d]

on behalf of the CALET Collaboration

[a] *Department of Physical Sciences, Earth and Environment, University of Siena, via Roma 56, 53100 Siena, Italy*

[b] *INFN Sezione di Pisa, Polo Fibonacci, Largo B. Pontecorvo, 3, 56127 Pisa, Italy*

[c] *Waseda Research Institute for Science and Engineering, Waseda University, 17 Kikuicho, Shinjuku, Tokyo 162-0044, Japan*

[d] *JEM Utilization Center, Human Spaceflight Technology Directorat, Japan Aerospace Exploration Agency, 2-1-1 Sengen, Tsukuba, Ibaraki 305-8505, Japan*

E-mail: francesco.stolzi@unisi.it, caterina.checchia2@unisi.it, bigongiari2@unisi.it, yakaike@aoni.waseda.jp

The Calorimetric Electron Telescope (CALET), in operation on the International Space Station since 2015, collected a large sample of cosmic-ray over a wide energy interval. Approximately 20 million triggered events per month are recorded with energies > 10 GeV. The instrument identifies the charge of individual elements up to nickel and beyond and, thanks to a homogeneous lead-tungstate calorimeter, it measures the energy of cosmic-ray nuclei providing a direct measurement of their spectra. Iron and nickel spectra are a low background measurement with negligible contamination from spallation of higher mass elements. Iron and nickel nuclei play a key role in understanding the acceleration and propagation mechanisms of charged particles in our Galaxy. In this contribution a direct measurement of iron and nickel spectra, based on more than five years of data, are presented in the energy range from 10 GeV/n to 2 TeV/n and from 8.8 GeV/n to 240 GeV/n, respectively. The spectra are compatible within the errors with a single power law in the energy region from 50 GeV/n to 2 TeV/n and from 20 GeV/n to 240 GeV/n, respectively. Systematic uncertainties are detailed and the nickel to iron flux ratio is presented. This unprecedented measurement confirms that both elements have very similar fluxes in shape and energy dependence, suggesting that their origin, acceleration, and propagation might be explained invoking an identical mechanism in the energy range explored so far.

41st International Conference on High Energy physics - ICHEP2022
6-13 July, 2022
Bologna, Italy

*Speaker

PoS(ICHEP2022)079

1. Introduction

The CALorimetric Electron Telescope (CALET) [1] is a space-based instrument installed on the International Space Station (ISS) on August 2015. It is optimized for the measurement of the all-electron spectrum [2, 3], but thanks to its large dynamic range, adequate calorimetric depth, accurate tracking, and excellent charge identification, CALET can also measure the flux of individual chemical elements in cosmic rays (CR) from proton to nickel in the energy range up to ∼1 PeV, searching for possible spectral hardening similar to the one already observed in the proton, carbon and oxygen spectra [4, 5]. In this paper, we describe the analysis procedure for iron and nickel fluxes measurement and present the energy spectra from 10 GeV/n to 2.0 TeV/n and from 8.8 to 240 GeV/n, respectively.

2. CALET instrument

CALET is an all-calorimetric instrument made of a CHarge Detector (CHD), a finely segmented pre-shower IMaging Calorimeter (IMC), and a Total AbSorption Calorimeter (TASC). The particle's energy is measured with the TASC, a lead-tungstate homogeneous calorimeter of 27 radiation lengths and 1.2 proton interaction lengths. The CR particle direction is reconstructed by IMC, made of 16 layers of thin scintillating fibers read out individually. The charge is identified by the CHD, a two-layered hodoscope of plastic scintillator paddles. It can resolve individual elements from atomic number Z = 1 to Z = 40 with excellent charge resolution. An independent charge measurement, via multiple samples of specific energy loss *(dE/dx)* in each fiber is also provided by IMC up to the onset of saturation which occurs for ions with higher charge than silicon. Therefore charge identification for nickel and iron relies on CHD only. Calibration and test of the instrument took place at the CERN-SPS during five campaigns between 2010 and 2015 with beams of electrons, protons, and relativistic ions. The TASC response was studied at CERN SPS in 2015 using a beam of accelerated ion fragments with A/Z = 2 and kinetic energy of 13, 19 and 150 GeV/c/n [6]. The mean energy released in the TASC is ∼20% of the particle energy and the resolution is ∼30%. The energy response of TASC turned out to be linear up to the maximum particle energy of 6 TeV obtained with a primary beam of ^{40}Ar nuclei. Monte Carlo (MC) simulations, reproducing the detailed detector configuration, physical processes, as well as detector signals are based on the EPICS simulation package[7]. Independent simulations based on FLUKA [8] and GEANT4 [9] are used to assess the systematic uncertainties for iron and nickel, respectively.

3. Data Analysis

The flight data (FD) used in the present analysis for iron (nickel) were collected over a period of 1613 (2038) days of CALET operation. The total observation live time for the high-energy (HE) shower trigger is $T \sim 3.3 \times 10^4$ h for iron and $T \sim 4.1 \times 10^4$ h for nickel. The HE trigger is based on the coincidence of the summed signals of the last four IMC layers and the top TASC layer (TASCX1). Each channel of CHD, IMC and TASC is calibrated using penetrating proton and He particles, selected in-flight by a dedicated trigger mode. Raw data are corrected for gain differences among the channels, light output nonuniformity, and any residual dependence on time

and temperature. After calibration, a track is reconstructed for each CR particle and each event is associated with an estimate of its charge and an energy. The incident CR track is found and fitted by a tracking algorithm based on a combinatorial Kalman filter fed with the coordinates provided by the scintillating fibers in the IMC. The angular resolution and the spatial resolution for the impact point on the CHD are $\sim 0.08°$ and $\sim 180\,\mu$m , respectively both for iron and nickel. Events with a well-fitted primary track crossing the detector from CHD top to TASC bottom and clear from the edges of TASCX1 and of the bottom TASC layer by at least 2 cm are used for iron analysis. No conditions on the last TASC layer is used for nickel analysis. The fiducial geometrical factors result $S\Omega \sim 416\,\mathrm{cm}^2\mathrm{sr}$ for iron and $S\Omega \sim 510\,\mathrm{cm}^2\mathrm{sr}$ for nickel. Since the HE trigger is fully efficient (close to 100%) for elements heavier than oxygen, an off-line trigger confirmation, as required for the analysis of lower charge elements [4, 5] is not necessary for this analysis. However, in order to select interacting particles, a deposit larger (by 2 sigmas) than the minimum ionization particle (MIP) peak is required in at least one of the first four layers of the TASC (shower event cut). The particle's charge Z is reconstructed from the signals of the CHD paddles traversed by the incident particle and properly corrected for its path length. Either CHD layer provides an independent dE/dx measurement which is corrected for the quenching effect in the scintillator's light yield. Two charge values (Z_{CHDX}, Z_{CHDY}) are reconstructed. The CHD charge resolutions σ_Z , obtained by combining the average of the Z_{CHDX} and Z_{CHDY} signal are $0.35e$ and $0.39e$ (in charge units) for iron and nickel, respectively as shown in [10, 11]. The residual background due to charge-changing nuclear interactions occurring in the upper part of the instrument are removed by requiring that the difference between the charges from either layer of the CHD is less than $1.5e$. Iron (nickel) candidates are selected by an ellipse centered on the nominal charge values (Z = 26, 28) with $1.25\,(1.4)\sigma_x$ and $1.25\,(1.4)\sigma_y$ wide semiaxes for Z_{CHDX} and Z_{CHDY}, respectively, and rotated clockwise by 45°. Following the aforementioned cuts, 5.2×10^3 Ni and 4.1×10^4 Fe candidate events are identified. For the flux measurement energy unfolding is applied to correct E_{TASC} distributions for bin-to-bin migration effects, due to the limited energy resolution, and infer the primary particle energy. The energy spectrum is obtained from the unfolded energy distribution as follows:

$$\Phi(E) = \frac{N(E)}{\Delta(E)\epsilon(E)S\Omega T}$$

$$N(E) = U[N_{obs}(E_{TASC}) - N_{bg}(E_{TASC}))]$$

where $S\Omega$ and T are the geometrical factor and the live time respectively, $\Delta(E)$ denotes the energy bin width, E is the geometric mean of the lower and upper bounds of the bin, $N(E)$ is the bin content in the unfolded distribution, $\epsilon(E)$ is the total selection efficiency [10, 11], $U()$ is the unfolding procedure operator, $N_{obs}(E_{TASC})$ is the bin content of observed energy distribution (including background), and $N_{bg}(E_{TASC})$ is the bin content of background events in the observed energy distribution. Background contamination from different nuclear species misidentified as Fe is $< 1\%$ in the energy range between 10^2 and 10^3 GeV of E_{TASC} increasing up to $\sim 2\%$ at $E_{TASC} \sim 10^4$ GeV. Background contamination for Ni is similar to that of Fe up to 10^3 GeV and it increases up to 10% at $\sim 10^4$ GeV .

4. Systematics errors

The most important sources of systematics uncertainties in the Fe and Ni analysis are due to charge identification and MC model. The systematic error related to charge identification was studied by varying the semi-minor and major axes of the elliptical selection up to 15%. That results in a flux variation depending on the energy bin, lower than 4% below 100 GeV/n for nickel, and lower than a few percent below 600 GeV/n for iron. Since it is not possible to validate MC simulations with beam test data in the high-energy region, a comparison between different MC models, i.e. EPICS and FLUKA for Fe and EPICS and GEANT4 for Ni, was performed. It is found that the total selection efficiencies for Fe and Ni determined with the two couple of models are in agreement within few percent over the whole energy range, but the energy response matrices differ by more than 5% in the low and high energy regions. The resulting fluxes show maximum discrepancies of 10% below 40 GeV/n (Fe) and 10% in the 100 – 200 GeV/n region (Ni). The uncertainty on the energy scale correction is ±2% and causes a rigid shift of the measured energies, affecting the absolute flux normalization by $^{+3.3}_{-3.2}$%(±4%) for Fe (Ni), but not the spectral shape. The uncertainties due to the unfolding procedure were evaluated with different response matrices computed by varying the spectral index (between −2.9 and −2.2) of the MC generation spectrum. The contributions due to the beam test model (not identical to the instrument now in orbit) and the shower event cut were evaluated and included in the systematic uncertainties. The systematic uncertainty due to off-acceptance events, tracking efficiency, background contamination and HE trigger efficiency are negligible both for iron and nickel. The fraction of interactions in the CHD, and above it, is checked by comparing the MC and the FD as explained in [10, 11]. The systematic error related to the atomic mass of nickel isotope composition (in this analysis, only the ^{58}Ni isotope was considered) reduces the normalization by 2.2%. Energy-independent systematic uncertainties affecting the fluxes normalization include live time (3.4%), long-term stability (< 2%), and geometrical factor (∼ 1.6%). The total systematic error is computed as the quadrature sum of all the sources of systematics in each energy bin.

5. Results

The energy spectra of Ni and Fe measured with CALET are shown in Fig. 1. Both spectra turn out to be consistent with most of the previous measurements within the uncertainty error band, both in spectral shape and normalization. Fig. 2 (Fig. 3) shows a fit to the CALET Fe (Ni) flux with a single power law (SPL) function from 50 (20) GeV/n to 2000 (240) GeV/n. The fit gives a spectral index $\gamma = -2.60 \pm 0.02$(stat) ±0.02(sys) with $\chi^2/d.o.f = 4.2/14$ for Fe and $\gamma = -2.51 \pm 0.04$(stat) ±0.06(sys) with $\chi^2/d.o.f = 0.3/3$ for Ni . The spectral index γ is also calculated for Fe by a fit of $d[log(\phi)]/d[log(E)]$ inside a sliding window centered in each energy bin and including the neighboring ±3 bins, in the region between 50 GeV/n and 2 TeV/n. The result in Fig. 4 shows that the Fe flux, in the fit region, is compatible within the errors with a single power law. The CALET nickel to iron ratio is shown in Fig. 5: it extends the results of previous experiments (i.e., HEAO3-C2) up to 240 GeV/n. The fit, performed from 8.8 to 240 GeV/n, gives a constant value of 0.061 ± 0.001(stat) with the $\chi^2/d.o.f. = 2.3/6$.

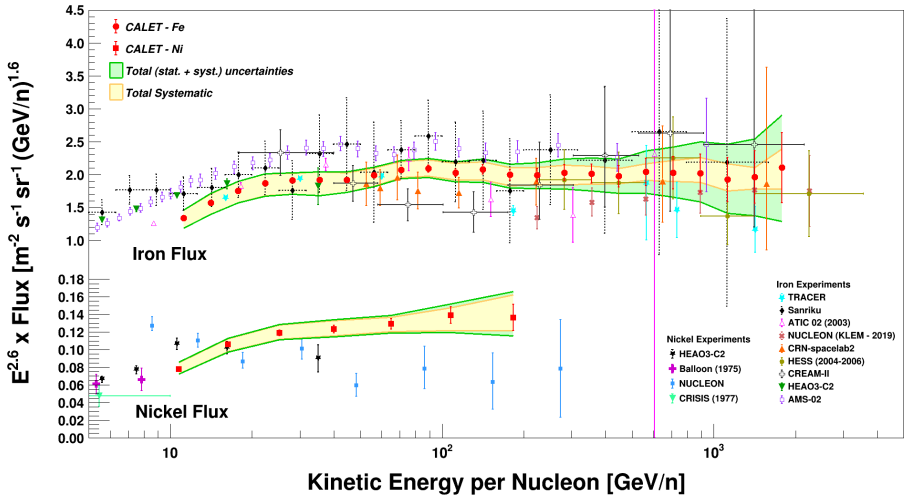

Figure 1: CALET Fe and Ni fluxes (multiplied by $E^{2.6}$) as a function of kinetic energy per nucleon. The error bars of the CALET data (red) represent the statistical uncertainty only, the yellow band indicates the quadrature sum of systematic errors, while the green band indicates the quadrature sum of statistical and systematic errors. Also plotted are other direct measurements. [12–23]

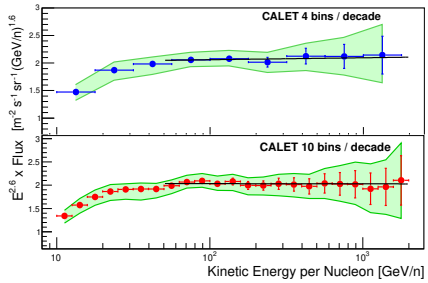

Figure 2: Fit of the CALET Fe energy spectrum to a SPL function (black lines) in the energy range [50, 2000] GeV/n with 4 bins/decade (top) and 10 bins/decade (bottom).The green band indicates the quadrature sum of statistical and systematic errors.

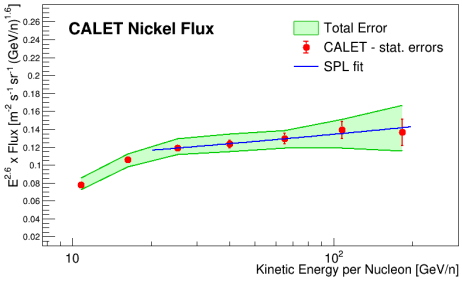

Figure 3: Fit of the CALET Ni energy spectrum to an SPL function (blue line) in the energy range [20, 240] GeV/n. The flux is multiplied by $E^{2.6}$ where E is the kinetic energy per nucleon. The error bars are representative of purely statistical errors

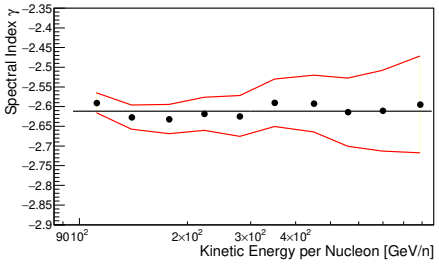

Figure 4: Energy dependence of the spectral index calculated within a sliding energy window for the CALET Fe data.The fit with a constant function (black line) gives a mean spectral index value $\langle\gamma\rangle = -2.61 \pm 0.01$.

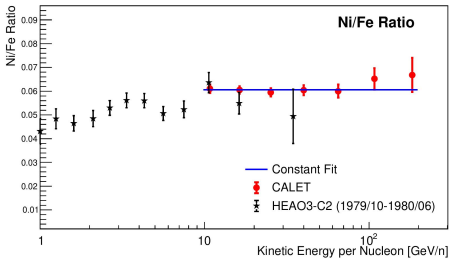

Figure 5: Ni to Fe flux ratio measured with CALET (red points). The errors bars are representative of statistical errors only. Data are fitted with a constant function giving Ni/Fe = 0.061 ± 0.001. Also plotted is the result from HEAO3-C2 [18].

6. Conclusion

We report a measurement of the energy spectra of iron and nickel from 10 GeV/n to 2.0 TeV/n and from 8.8 to 240 GeV/n, respectively with a significantly better precision than most of the existing

measurements. Between 50 (20) GeV/*n* and 2000 (240) GeV/*n* Fe (Ni) spectrum is consistent with the hypothesis of a SPL with a spectral index $\gamma = -2.60 \pm 0.03$ ($\gamma = -2.51 \pm 0.07$), however, beyond this limit, the statistical and systematic uncertainties do not allow us to draw a significant conclusion on a possible deviation from a single power law. The flat behavior of the Ni to Fe ratio suggest that both elements have very similar fluxes in shape and energy dependence, suggesting that their origin, acceleration, and propagation might be explained invoking an identical mechanism in the explored energy range.

References

[1] S. Torii and P.S. Marrocchesi *Adv. Space Res.* **64** (2019) 2531.

[2] O. Adriani et al. *Phys. Rev. Lett.* **119** (2017) 181101.

[3] O. Adriani et al. *Phys. Rev. Lett.* **120** (2018) 261102.

[4] O. Adriani et al. *Phys. Rev. Lett.* **122** (2019) 181102.

[5] O. Adriani et al. *Phys. Rev. Lett.* **125** (2020) 251102.

[6] Y. Akaike in *Proceedings of Science (ICRC2015) 613*, 2015.

[7] See EPICS webpage http://cosmos.n.kanagawa-u.ac.jp/EPICSHome/.

[8] T.T. Böhlen et al. *Nuclear Data Sheets* **120** (2014) 211.

[9] J. Allison et al. *Nucl. Instrum. Methods Phys. Res., Sect. A* **835** (2016) 186.

[10] O. Adriani et al. *Phys. Rev. Lett.* **126** (2021) 241101.

[11] O. Adriani et al. *Phys. Rev. Lett.* **128** (2022) 131103.

[12] A. Panov et al. *Bull. Russian Acad. Sci.* **73** (2009) 564.

[13] M. Ave et al. *Astrophys. J.* **678** (2008) 262–273.

[14] H.S. Ahn et al. *Astrophys. J.* **707** (2009) 593.

[15] V. Grebenyuk et al. *Adv. in Space Res.* **64** (2019) 2546.

[16] M. Ichimura et al. *Phys. Rev. D* **48** (1993) 1949.

[17] F. Aharonian et al. *Phys. Rev. D* **75** (2007) 042004.

[18] J.J. Engelmann et al. *Astron. Astrophys.* **233** (1990) 96.

[19] D. Müller et al. *Astrophys. J.* **374** (1991) 356.

[20] M. Aguilar et al. *Phys. Rev. Lett.* **126** (2021) 041104.

[21] G. Minagawa *Astrophys. J.* **248** (1981) 847.

[22] J.S.Young et al. *Astrophys. J.* **246** (1981) 1014.

[23] V. Grebenyuk et al. *arXiv:1809.07285 [astro-ph.HE]* (2018) .